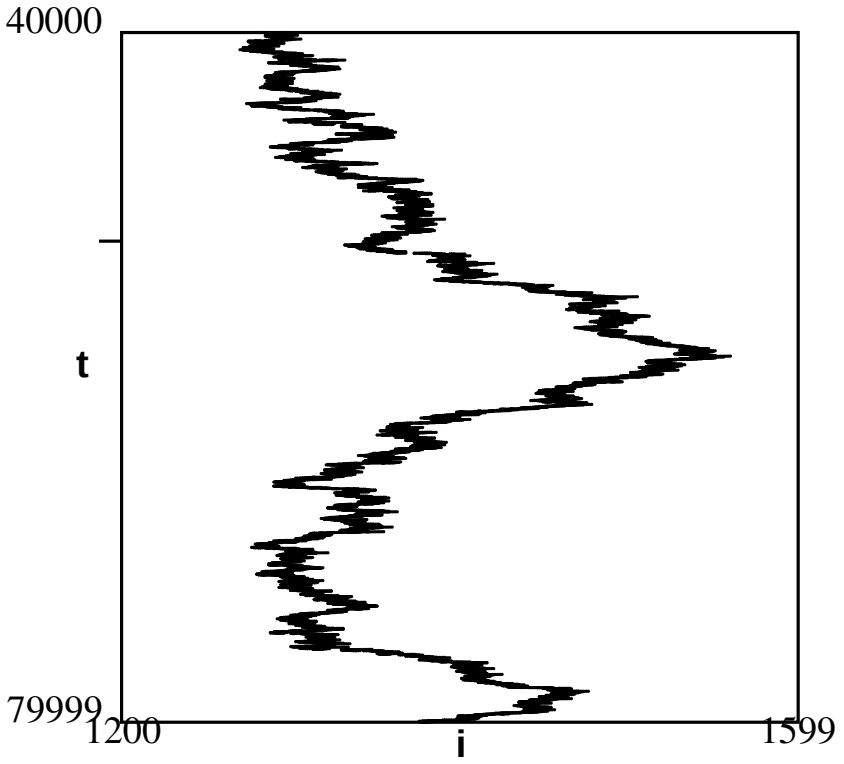

Fig. 15. Expanded view of a part of Fig. 14. Every iteration is displayed. The tick mark at $t = 52000$ shows the location of Fig. 16. The apparent break in the trajectory just below that point shows the recognized dislocation making a large lateral jump to the right in a single time step.

The plume's width $\sigma(t) \equiv \left\langle x^2 \right\rangle^{1/2}$, plotted against time in Fig. 19, quickly approaches the time dependence of a random walk. As the straight line in Fig. 19 indicates, we find $\sigma(t) \approx (2Dt)^{-\alpha}$ with a least-squares fit for $t > 512$ giving $D = 0.506$ and $\alpha = 0.501 \pm 0.004$. The systematic deviation from Gaussian diffusion seen at early times is again due to the recognition asymmetry, which gives $2^{-i/2}$ tails to the distribution and to the binomial structure of the dislocation movement. The result of the exact analysis of these effects is that, for example, $\log \sigma(1) = 3/2$. The simulations give $\log \sigma(1) = 1.52 \pm 0.05$.

To complete the statistical analysis of rule 18 diffusion dynamics facilitated by the dislocation detection transducer, we remeasure the temporal decay rate of the dislocation number density. Grassberger[23] estimated it using a rarefied dislocation gas on a very large lattice; that is, initial patterns with widely separated dislocations of the form $(\Sigma 0)^* 11 (0\Sigma)^*$. Additionally, dislocations after $t = 0$ were detected only as isolated pairs of 1's; i.e. as $(\Sigma 0)^* 11 (0\Sigma)^*$ again. Thus, dislocations were not counted in any other form, such as $(\Sigma 0)^* 10^{2n} 1 (0\Sigma)^*, n = 1, 2, \ldots$. The consequence is that statistics could only be gathered relatively infrequently and for a limited type of initial ensemble. Here we avoid these problems entirely and collect substantially better

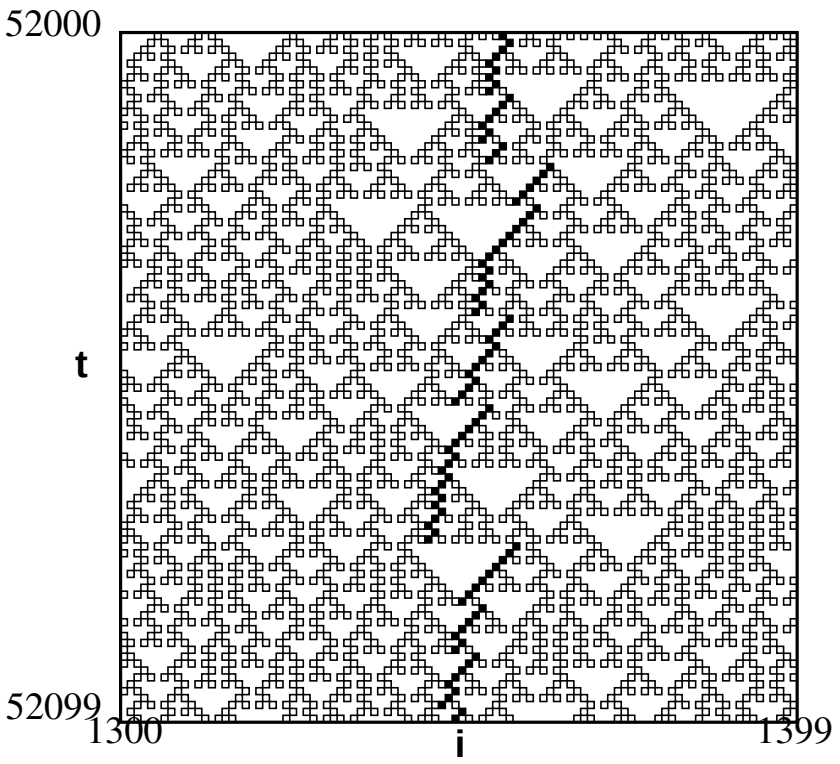

Fig. 16. Trajectory of a single dislocation recognized by $\mathrm{T}_{\mathtt{domain}}(\Lambda^0)$. This is an expanded view of a part of Fig. 15, located at the tick mark on the vertical axis of that figure. The region shown is in fact smaller than the width of the tick.

statistics on unrestricted initial conditions by using the domain metric to estimate the dislocation number density

$$d_N(t) = N^{-1}\|\Phi_t(\mathbf{s})\|_{\mathrm{M}(\Lambda^0)}$$

We count the density $d_N(t)$ of dislocations at each time in a randomly-generated state $\mathbf{s}_0 \in \mathcal{A}^N$. The result is graphed in Fig. 20, where we see $d_{10^5}(t)$ plotted against time. As the straight line suggests, we find $d(t) = (8\pi D)^{-1/2}t^{-\alpha}$ with least-squares analysis giving values of $D = 0.54$ and $\alpha = 0.49 \pm 0.04$. The estimate is from a fit over data at all times.

Finally, we briefly mention the vicinity convergence properties. The fraction of vicinity patterns of Λ^0, say, that have not been attracted to Λ^0 after t steps on an N-site lattice is given by

$$f(N,t) = \frac{\left\|\widehat{V}_t^0(N)\right\|}{\|V^0(N)\|}$$

where $\widehat{V}_t^0 = \mathbf{\Phi}_t\big(V^0\big) - \Lambda^0$. We estimate this statistic via a Monte Carlo sample of V^0. There are two results of immediate use. First, on even-size lattices up to 500 sites we found an

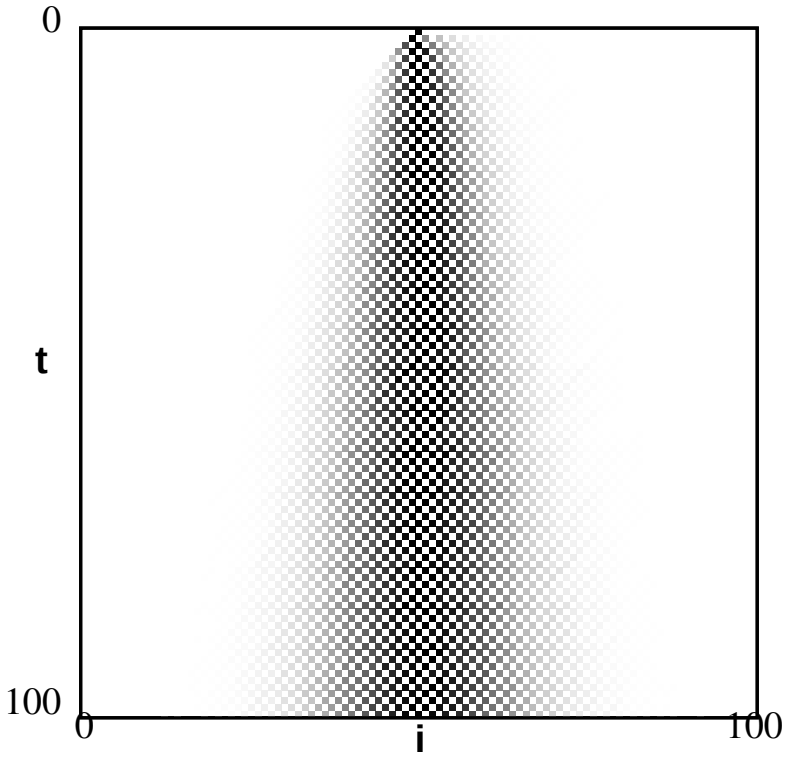

Fig. 17. The dislocation plume: Evolution of the initial ensemble $\Lambda^{0,0}$ consisting of configurations with a single dislocation. The gray scale intensity of a space-time cell is proportional to the number of dislocations visiting there. It is normalized at each time step to run from white to black so the distribution tails are more apparent.

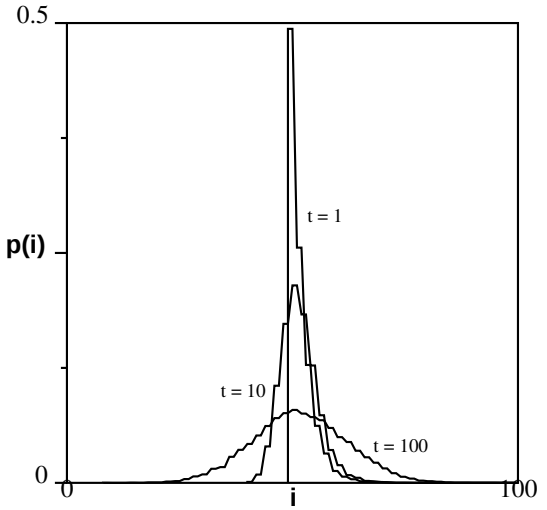

Fig. 18. Dislocation histogram at times $t = 1,\ 10,$ and 100.

upper bound $f_{\max}(N, \infty) \propto N^{-\gamma}$ with $\gamma = 0.51 \pm 0.02$, using 20,000 initial vicinity patterns.